Diverse response of global terrestrial vegetation to astronomicalforcing and CO_2 during the MIS-11 and MIS-13 interglacials

Qianqian Su[1#], Anqi Lyu[1#], Zhipeng Wu[1,2,3], Qiuzhen Yin[1*]

[1]George Lemaitre Centre for Earth and Climate Research, Earth and Life Institute, Université catholique de Louvain, Louvain-la-Neuve, Belgium

[2]Key Laboratory of Cenozoic Geology and Environment, Institute of Geology and Geophysics, Chinese Academy of Sciences, Beijing, China

[3]University of Chinese Academy of Sciences, Beijing, China

[#]Qianqian Su and Anqi Lyu contributed equally to this paper.

*Corresponding author: Qiuzhen Yin (qiuzhen.yin@uclouvain.be)

Abstract

Disentangling the links between terrestrial vegetation changes and astronomical forcing as well as CO_2 is of great help to understand the sensitivity of contemporary vegetation and predict future vegetation and climate changes, yet it remains challenging. Given the distinct differences in astronomical configurations and CO_2 concentration between Marine Isotope Stage (MIS) 11 and 13, here we investigate the role of astronomical forcing and CO_2 on global vegetation changes during these two interglacials based on transient simulations performed with the model LOVECLIM1.3. Our results show that during these two interglacials, astronomical forcing plays a dominant role on the vegetation evolution, with the effect of CO_2 being relatively small. The effect of astronomical forcing on vegetation can be explained successively by the relationship between climate (temperature, precipitation) and the astronomical parameters and by the relationship between vegetation and climate. The relative effect of precession and obliquity on vegetation strongly depends on regions and on interglacials. In general, obliquity plays a more important role on vegetation variations during MIS-11, while precession is more important during MIS-13. Our results also reveal a clear half-precession cycle (~10 ka) in the variations of temperature, precipitation and vegetation in the tropical area during MIS-13, as a direct response to the tropical insolation. However, no obvious half-precession cycle is simulated during MIS-11 due to its weak precession variation but large obliquity variation, indicating that half-precession cycle is not stable in time.

Key words: Interglacials, MIS-11, MIS-13, paleoclimate modelling, precession, obliquity, vegetation

1. Introduction

The spatial distribution of major vegetation types on the globe is primarily controlled by climatic variables (e.g. temperature, precipitation) and internal feedbacks. The variations of insolation and atmospheric CO_2 concentration are important factors influencing climate, and then on the vegetation's spatial and temporal variations. The latitudinal and seasonal distribution of insolation is determined by three astronomical parameters: eccentricity, climatic precession and obliquity (Berger 1978). Sufficient insolation changes caused by these parameters' variations significantly affect climate and vegetation (e.g. Harrison et al. 1995; Crucifix et al., 2005a, 2005b; Tzedakis et al., 2004, 2006; Claussen et al. 2006; Fletcher and Sánchez Goñi, 2008; Sánchez Goñi et al., 2008, 2016).

During the last decade, the generation of long and high-resolution pollen records from terrestrial and marine sediments with improved chronological controls has provided insights into the relationship between vegetation and climate variability as well as astronomical parameters. For example, high-resolution pollen analysis revealed the influence of precession on forest development and vegetation composition in the western Mediterranean basin over the last 48 ka (Fletcher and Sánchez Goñi, 2008). Vegetation changes over the past 300 ka from South Africa are found to be driven by precessional forcing through its impact on rainfall distribution and seasonality (Dupont et al. 2022). The variations of the tree population in southern Europe have been found to respond to insolation on orbital and suborbital scales during the glacial-interglacial cycles over the last 450 ka (Tzedakis 2005). Zhao et al. (2020) and Sun et al. (2019) investigated the varied roles of astronomical forcing and ice/CO_2 in the evolution of climate and vegetation across the mid-Pleistocene transition based on the long-term records on the Tibetan Plateau and the Chinese Loess Plateau, respectively. The paleoclimate and vegetation reconstructions during the Mid-Pliocene reflect the impact of increased CO_2 concentrations and the effect of orbital forcing (Willeit et al. 2013). Bonis et al. (2010) found that spore peaks could be related to precession-induced variations in monsoon strength at the Triassic-Jurassic transition. In addition to vegetation reconstructions, Dynamic Global Vegetation Models (DGVMs) and integrated Earth system models (ESMs) have also been used to investigate the interactions between climate, insolation, atmospheric CO_2 and vegetation, such as the individual and combined effects of astronomical parameters and CO_2 on the differentiated regional vegetation (Crucifix and Loutre 2002; Tuenter et al. 2003; Jiménez-Moreno et al. 2007; Yin and Berger 2012; Bounceur et al. 2015).

The past interglacials provide the opportunity to investigate the vegetation response to different forcing and the related feedbacks under warm climate conditions, which could help us further understand the sensitivity of contemporary vegetation and predict future vegetation and climate changes. Previous studies show that the response of vegetation could be very different between interglacials and among different regions (Brovkin 2002; Granoszewski et al. 2005; Tarasov et al. 2007; Tarasov et al. 2009; Giesecke et al. 2011; Yin and Berger 2012; Zhao et al. 2014; Rachmayani et al. 2015; Dallmeyer et al. 2021).

Marine Isotope Stage 11 (MIS-11), an interglacial about 400 ka ago, has been paid special attention in paleoclimate studies. This is mainly because (1) MIS-11 was one of the warmest and longest (~30 ka) interglacials characterized by the highest amplitude deglacial warming of the last million years with the highest stand sea level (Droxler and Farrell 2000; Masson-Delmotte et al. 2010; Lang and Wolff 2011; Raymo and Mitrovica 2012; Coletti et al. 2015; Dutton et al. 2015), and (2) MIS-11 had been highlighted as an analogue of the present interglacial (MIS-1) due to its similar astronomical configurations (mainly low eccentricity), high atmospheric CO_2 concentrations, mean climate state and degree of stability with the Holocene (Loutre and Berger 2003; Mcmanus et al. 2003; Lüthi et al. 2008; Tzedakis 2010; Yin and Berger 2015). Several studies aim at presenting vegetation/climate evolution during MIS-11 based on proxy records from different sites, including Lake Baikal (Prokopenko et al. 2009; Shichi et al. 2009), Lake El'gygytgyn in Northeast Russia (Tarasov et al. 2013; Vogel et al. 2013), Southwestern Europe (Oliveira et al. 2016) and Northwest Africa (Helmke et al. 2008). These studies provide a view on specific climate or vegetation evolution sequences at regional scale during MIS-11. Model simulations are also applied to study climate and vegetation changes during MIS-11. For example, Oliveira et al. (2018) compared the controlling factors of vegetation in MIS-11 and MIS-19 with MIS-1 in Southwest Europe and revealed that the forest dynamics were mostly coupled to changes in winter precipitation which is mainly controlled by precession, with CO_2 playing a minor role. Kleinen et al. (2014) compared two model results and proxy-based climate/vegetation reconstructions for different time slices in MIS-11 at global and regional scales, and addressed that different climate states could exist during one interglacial.

In contrast to MIS-11, MIS-13, the interglacial just preceding MIS-11 and occurring about 500 ka ago, was the most glaciated and coolest interglacial globally speaking over the last million years. However, some studies show that MIS-13 was not a weak interglacial in some regions in the Northern Hemisphere, including vegetation reconstructions (Tzedakis et al. 2006; Yin and Guo 2006; Yin and Guo 2008; Guo et al. 2009; Markovic et al. 2009; Prokopenko et al. 2009; Markovic et al. 2012). Based on pollen records or plant macrofossils, the vegetation changes during MIS-13 have been revealed at regional scale, such as in Italy (Russo Ermolli et al. 2015), in Poland (Stachowicz-Rybka 2015) and in southern Europe (Margari et al. 2018; Oliveira et al. 2020), which show that MIS-13 is not necessarily a weak interglacial as compared to MIS-11 in terms of arboreal pollen abundance. Model simulations show that extremely asymmetrical polar ice sheets could induce strong East Asian summer monsoon during MIS-13 (Shi et al. 2020). The reconstructions from various sites reveal different magnitudes and phase patterns of regional climate and vegetation evolution in MIS-11 and MIS-13, characterized by distinct durations of climate optima and distinct timing of major shifts. However, systematical analyses of the global patterns of the correlation between vegetation and astronomical forcing as well as the difference between the two interglacials are rare.

The astronomical configurations of MIS-11 and MIS-13 are very different (Fig. 1), leading to different latitudinal and seasonal distribution of insolation (Yin and Berger 2012). MIS-11 is characterized by a relatively small variation in precession due to its small eccentricity, but a large variation of obliquity. It has an atmospheric CO_2 concentration of about 280 ppmv, which is quite close to the Holocene level. However, MIS-13 is characterized by a large variation of precession due to a large eccentricity but smaller variation in obliquity, and has a lower CO_2 concentration (about 240 ppmv). Given these differences in forcings between MIS-11 and MIS-13 and in their background global climate conditions, in this study we compare the response of vegetation to the astronomical forcing and CO_2 between the two interglacials based on model simulations, with the following questions in mind:

(1) What is the relative influence of precession and obliquity as well as CO_2 on global vegetation distribution during these two interglacials?
(2) What are the fundamental differences between the two interglacials in global vegetation variations?

For this purpose, we performed transient simulations for MIS-13 and MIS-11 with the model LOVECLIM 1.3, where a dynamic vegetation model (VECODE) is included. This paper is organized as follows. Section 2 describes the model and the experiments setup. In Section 3, we explore the influence of astronomical parameters and CO_2 on vegetation during MIS-11 and MIS-13 (Section 3.1, 3.2, 3.3 and 3.4) and the half-precession signals (Section 3.5). Conclusions are given in Section 4.

2. Model and experiments setup

The simulations used in this study are those performed in Yin et al. (2021) with the model LOVECLIM 1.3. The detailed information of the model and experiment design are given in their study. Here we only briefly introduce the model and experiments with more information on the vegetation component in the model. A previous version LOVECLIM 1.2 is described in detail in Goosse et al. (2010). It is a three-dimensional Earth system model of intermediate complexity. In the version we used, atmosphere (ECBilt), ocean-sea ice (CLIO) and terrestrial biosphere (VECODE) are interactively coupled, ice sheets and ocean carbon cycle being prescribed to their present-day configuration. A detailed description of each component and its coupling can be found in Goosse et al. (2010).

VECODE (VEgetation COntinuous DEscription model), is a reduced-form DGVM that simulates changes in vegetation structure and terrestrial carbon pools on timescales ranging from decades to millennia (Brovkin et al. 1997). The shortest time step is 1 year. Two primary plant functional types (PFTs), tree and grass, using the fractional bioclimatic classification, are identified as the vegetation cover in each land grid cell. The tree fraction (F_{tree}) is represented as a function of climate (annual mean precipitation and the growing degree days above 0 (GDD0)). Semi-empirical parameterizations based on the regularities of distribution of forest and desert in climatic space (Lieth, 1975) and the climate dataset of Leemans and Cramer (1991) and Olson and Watts (1992) which describes the correspondence between climate and vegetation were used for the F_{tree} and the desert fraction (F_{desert}) computations (Brovkin et al., 19997; Goosse et al., 2010). After the computation of F_{tree} and F_{desert}, the rest of the grid cell is covered by grass, F_{grass} = 1- F_{tree} - F_{desert}. The sum of F_{tree} and F_{grass} equals the vegetation fraction (F_{veg}). In the VECODE version used in this study, the vegetation fraction evolution is climate dependent only (annual mean precipitation and GDD0), without the effect of CO_2 fertilization nor leaf area on vegetation fraction. For any given climate, there is a unique stable composition of PFTs corresponding to the climate. If climate changes, then the vegetation model simulates the transition from the equilibrium for the previous climate to a new equilibrium with the new climate. Studies have revealed that despite the simplicity of its climate and the vegetation features, VECODE simulated basic global patterns qualitatively well and in good correspondence with data of present-day observations and paleo-proxy reconstructions as well as results from more complex dynamic global vegetation models (Cramer et al. 2001).

To investigate the impact of insolation and CO_2 on climate and vegetation, two sets of transient simulations were performed for each of MIS-13 and MIS-11, and the simulation periods are from 538 to 471 ka BP for MIS-13 and 424 to 382 ka BP for MIS-11. The three astronomical parameters and the CO_2 concentration during the simulation periods are shown in Fig. 1. In the first set of simulations, the initial conditions are provided by a 2000-year equilibrium run with the pre-industrial greenhouse gases (GHGs) values (CO_2 = 280 ppmv, CH_4 = 760 ppbv, N_2O = 270 ppbv) and the astronomical parameters (Berger and Loutre 1991) at the starting date of the simulated period. Then we conducted the transient run with time-varying insolation and the pre-industrial GHGs. This experiment, denoted hereafter as "Orb", allows investigating the impact of astronomical forcing alone under the pre-industrial GHG condition. In the second set of simulations, the initial conditions were obtained by a 2000-year equilibrium run using the GHGs and the astronomical parameters at the starting date of the simulated period. Then in the transient run, insolation and GHGs vary with time, denoted hereafter as "OrbGHG". Comparison between these two sets of experiments allows investigating the impact of GHGs.

3. Results

3.1 Simulated global distributions of tree, grass and desert under extreme astronomical conditions

In order to quantify the relative importance of precession and obliquity on regional vegetation distribution, multiple linear regression analysis was carried out between vegetation variations and precession and obliquity using the Orb experiment of MIS-11 (section 3.2) and the Orb experiment of MIS-13 (section 3.3). The precession parameter is defined by e sin ($\tilde{\omega}$), where e is eccentricity and $\tilde{\omega}$ is the longitude of the perihelion measured from the moving vernal point and the present-day value of $\tilde{\omega}$ is 102.04° (Berger, 1978; Berger et al., 2010). When $\tilde{\omega}$ = 0°, 90°, 180° and 270°, fall equinox, winter solstice, spring equinox and summer solstice is at perihelion, respectively. Therefore, precession minimum (when $\tilde{\omega}$ = 270°, sin ($\tilde{\omega}$) = -1) corresponds to high summer insolation in the Northern Hemisphere and precession maximum (when $\tilde{\omega}$ = 90°, sin ($\tilde{\omega}$) = 1) corresponds to low summer insolation in the Northern Hemisphere. In order to study the relationship between precession and climate from the perspective of insolation, the inverse value of precession (the original precession value multiplied by -1, denoted by -precession) is used in the regression analysis.

As shown in Brovkin et al (1997), the tree fraction in the major desert regions is close to zero. Hence, regression analysis for tree fraction over these regions would not make sense. The same happens for the regression analysis for grass fraction over the regions where grass fraction is close to zero. Therefore, before making any interpretation of the regression results, we first examine in our simulations the major regions where tree fraction is near zero and the regions where grass fraction is near zero to avoid unreasonable interpretations over these regions. As the area of these regions may vary with different astronomical configurations, we analyze the F_{tree}, F_{grass} and F_{desert} under four extreme astronomical conditions: maximum and minimum obliquity conditions (417 kaBP and 395 kaBP respectively) selected from the MIS-11 Orb simulation, and maximum and minimum precession conditions (496 kaBP and 506 kaBP respectively) from the MIS-13 Orb simulation.

Fig.2 shows that the large-scale distributions of tree, grass and desert are very similar between the four extreme obliquity and precession conditions. For all the four conditions, F_{tree} is less than 10% in the Arctic tundra region, in Central North America and Central South America, in East Europe and Central Asia, in the Sahara Desert and Arabian Peninsula, in Tibetan Plateau and East China, in Australia and western South Africa. Therefore, in these regions, the regression results for F_{tree} will not be discussed. Actually, in most of these regions except a few permanent desertic regions, the absence of tree is compensated by the occupation of grass. Similarly, in the regions dominated by tree, grass fraction is very low. Under the four conditions, in addition to Greenland and Antarctica, there are several regions that are always dominated by desertic condition, including Central Australia, Central South America, Tibetan Plateau and Central Asia. The regression results for both F_{tree} and F_{grass} over these regions will therefore be ignored in the following sections. Finally, the place where the vegetation distribution is the most sensitive to changes in precession and obliquity is in the Sahara region. Under maximum obliquity and minimum precession, both favoring high summer insolation in the Northern Hemisphere, almost the entire Sahara region is dominated by grass with very limited deserts and the tree distribution is also extended northward in North Africa. Under minimum obliquity and maximum precession, the Sahara Desert is enlarged and only the Sahel region is dominated by grass.

3.2 Influence of astronomical parameters on vegetation during MIS-11

Based on the relationship of the F_{tree} with -precession and obliquity, the global continental regions where the tree fraction is not near zero (section 3.1, Fig.2), can be divided into the following groups with each sharing similar characteristics (Fig. 3a, Table 1):

- In the Subarctic taiga region and the Mediterranean region, the F_{tree} has a positive correlation with both -precession and obliquity, and obliquity is more important than precession. The wavelet power spectrum analysis of pollen records from Tenaghi Philippon in the Mediterranean also demonstrates a stronger obliquity signal (Tzedakis et al. 2006).
- In Southern Asia and East Africa, the F_{tree} has a positive correlation with both -precession and obliquity, but precession is more important than obliquity.
- Over most areas of the mid-latitude continent interior, including the North American Monsoon region and the lands extending from Northeast China to Southwest Russia, the F_{tree} has a negative correlation with both -precession and obliquity, and obliquity is more important than precession.
- In South Africa monsoon region, the F_{tree} is negatively correlated with -precession and obliquity.
- In the northern South America, the F_{tree} is positively correlated with -precession but negatively correlated with obliquity.

Similar analysis has also been made for the F_{grass} (Fig. 3b) and the F_{veg} (Fig. 3c). The results for the F_{veg} are very similar to those of the F_{tree}, showing that the relationship between vegetation and the astronomical parameters are mainly determined by trees. As far as the relationship of F_{grass} with precession and obliquity is concerned, the regions dominated by grass (section 3.1, Fig.2) can be divided the following:

- In the Arctic tundra region, Central North America and Central South America, East Europe and Central Asia, Arabian Peninsula, East China, the F_{grass} is positively correlated with both the -precession and obliquity.
- In the Sahel region and North Australia, the F_{grass} is negatively correlated with both -precession and obliquity, and obliquity is more important than precession.

In our model, insolation influences vegetation mainly through its effect on annual mean precipitation and GDD0 as explained in section 2. Therefore, to better understand the relationships between vegetation and precession and obliquity, we need first to understand the relationship between vegetation and these two climate factors, and then to understand how these two factors respond to precession and obliquity.

We applied simple liner regression analysis to discover the relationship between vegetation and two climate factors, because precipitation and GDD0 are strongly correlated in many places (Fig. S1). Fig. 4a shows that the F_{tree} is significantly and positively correlated with annual precipitation almost everywhere, while GDD0 has a more diverse impact on the F_{tree} at regional scale. In the high latitudes of the Northern Hemisphere, where tree growth is strongly constrained by the number of days with the mean air temperature above 0°C (Hoegh-Guldberg et al. 2018), the F_{tree} is strongly and positively correlated with GDD0. In Southern Asia, the F_{tree} is strongly correlated with precipitation but its relationship with GDD0 is very weak. In the lands extending from Northeast China to Southwest Russia, F_{tree} is negatively correlated with GDD0. In most areas of the Southern Hemisphere, the impact of GDD0 on the F_{tree} is less obvious. Note that the strong correlation of F_{tree} with precipitation and GDD0 in some subtropical desertic regions such as the Sahara, the central Asia and Australia is not valid because the tree fraction is near zero in these regions.

It is worth noting that the influences of annual precipitation and GDD0 on the F_{grass} are similar to their influence on the F_{tree} in North Africa, inland Australia and some areas of temperate Eurasia. Over these regions, with F_{veg} lower than 50% even in the period with maximum boreal summer insolation (412 - 408 ka BP), the warm and humid climate favours the growth of any vegetation.

Regarding the relationships of the two climate factors with precession and obliquity, Fig. 5b shows that GDD0 is positively correlated with obliquity and -precession globally. Obliquity is more important in the mid and high latitudes, while precession is more critical in the low latitudes and over the Tibetan Plateau. This could be explained by the importance of obliquity on the annual irradiation in the mid-high latitudes in both hemispheres (Berger et al. 2010) and the dominant role of precession on the tropical climate (Pokras and Mix, 1987; Tuenter et al., 2003; Jahn et al., 2005; Kutzbach et al., 2008; Wu et al. 2020).

As precipitation has strong regional variability, only the regions where the absolute value of correlation coefficients between annual precipitation and the astronomical parameters greater than 0.4 are analyzed (Fig. 5a). In the high latitudes, obliquity and -precession both are in positive correlations with precipitation. High obliquity and -precession cause high summer insolation and then precipitation increase in this area (Yin and Berger 2012). In the mid-latitudes, -precession has a negative effect on precipitation in temperate North America. This is in agreement with a previous modelling study (Shin et al. 2006) which simulates a drier North America at the mid-Holocene when precession reaches the minimum. Data synthesis also shows a midcontinental drying during the mid-Holocene partially related to high summer insolation (Harrison et al. 2003; Williams et al. 2010). In Western Europe and Mediterranean Region, total annual precipitation is dominated by precipitation in winter, instead of growing seasons, while vegetation is controlled by precipitation during the growing season. Therefore, the relationship between annual mean precipitation and astronomical parameters cannot explain the relationship between F_{veg} and astronomical parameters. In northern China, precipitation is more sensitive to the -precession than obliquity. It is in line with the strong precession cyclicity of simulated mean annual precipitation during the last 0.7 Ma (Sun et al. 2019). In North African, Indian and East Asian monsoon regions, -precession has a positive influence on precipitation, whereas it has a negative impact on precipitation in the southern hemisphere monsoon regions, which is related to the meridional shift of the ITCZ (the Intertropical Convergence Zone) caused by insolation change. In Africa, obliquity has a strong positive influence in North African monsoon regions and Sahara and a negative influence in South Africa. A larger obliquity would lead to a stronger cross-equatorial insolation gradient and therefore a stronger cross-equatorial pressure gradient, which brings more southerly cross-equatorial winds into North Africa and Sahara, consequently decreasing the southern precipitation (Bosmans et al. 2015). Obliquity has a positive influence on precipitation in temperate Australia, which is similar to what has been found by Wyrwoll et al. (2007). They found that as obliquity increases, the equatorial belt turns colder, leading to a converging surface flow transporting towards the extratropic over both the continent and ocean and enhanced Australian monsoon rainfall. This can also explain why in South America, obliquity has a negative influence on the precipitation in tropical South America and a positive influence on extra-tropical South America.

In summary, how precession and obliquity influence the vegetation can be explained successively by the relationships between the astronomical parameters, the climate factors and vegetation, which are summarized in Table 1 and Table 2 for different regions.

Table 1 The relationship between GDD0, annual mean precipitation and the F_{tree} with -precession and obliquity during MIS-11 (in red) and MIS-13 (in blue) in the Orb simulations.

Orb F_{tree}	precipitation		GDD0		F_{tree}		F_{tree}	
	-precession	obliquity	-precession	obliquity	precipitation	GDD0	-precession	obliquity
Subarctic taiga region, Mediterranean	+	++	+	++	++	++	+	++
	++	+	+	+	++	++	++	+
South Asia and East Africa	++	+		+	++	+	++	+
	++	+		+	++		++	+
North American Monsoon region, Northeast China to Southwest Russia	-	-	+	++	++	--	-	--
	--		++	+	++	--	-	-
South Africa monsoon region		--	++	+	++		-	-
		--	++	+	++	-	-	-

northern South America	+	-	++	+	++	+	+	-
	+	-	++	+	++	++	+	-

The + and - stand for a positive and negative relationship, respectively. The blank stands for no significant relationship, or the process not involved in our explanation. Columns 2 to 5 show the relationship between annual mean precipitation, GDD0 and astronomical parameters. Columns 6 and 7 present the relationship between the F_{tree} and climate factors. The last two columns show the influence of astronomical parameters on vegetation. The regression coefficients higher than 0.6 or lower than -0.6 in each sub-region are indicated by ++ or --. The regression coefficients between -0.6 and 0.6 are indicated by + or -.

Table 2 Same as Table 1 but for the F_{grass}.

Orb F_{grass}	precipitation		GDD0		F_{grass}		F_{grass}	
	-precession	obliquity	-precession	obliquity	precipitation	GDD0	-precession	obliquity
Arctic tundra region	+	++	+	++	+	+	+	+
	+	+	+	+	+	+	+	+
Central North America	-	-	+	++	-	++	+	+
	--	-	++	+	-	+	+	+
East Europe and Central Asia	+	++	+	++	++	+	+	+
	++	+	+	++	++	+	++	+
Arabian Peninsula	+	++	+	++	+	++	+	+
	++	+		+	++		++	+
East China	++	+		+	++	+	++	+
	++	+		+	++		++	+
Sahel region	+	++	+	+	--	--	-	-
	++	+		+	++		--	-
North Australia	-	+	++	+	--	-	-	-
	--	-	++	+	++	--	-	-

3.3 Differences of astronomical influence on vegetation between MIS-13 and MIS-11

The comparison between Fig. 3a and Fig. 6a shows that the relationship of the F_{tree} with -precession and obliquity is obviously different between MIS-11 and MIS-13. The spatial distribution of the sign of the coefficients of both -precession and obliquity during MIS-13 is very similar to MIS-11, showing the robustness of the qualitative relationship of the F_{tree} with precession and obliquity. However, contrary to what is observed during MIS-11, precession plays a more important role than obliquity on the F_{tree} in Subarctic taiga region, Mediterranean region, South Asia and East Africa during MIS-13. Regarding the F_{grass}, the spatial distribution of the sign of the coefficients of both -precession and obliquity during MIS-13 (Fig. 6b) is also very similar to MIS-11 (Fig. 3b), and in some regions (East Europe and Central Asia, Arabian Peninsula, East China, Sahel region) precession also plays a more important role than obliquity on the F_{grass} during MIS-13.

The difference between MIS-11 and MIS-13 is anticipated if the difference in their astronomical conditions is considered. The large eccentricity during MIS-13 leads to a high-amplitude variation of precession, whereas the exceptionally low eccentricity during MIS-11 leads only to a small variation of precession (Fig. 1). In the meantime, the variation of obliquity during MIS-11 is larger than that during MIS-13. Thus, obliquity plays a more important role on the F_{tree} during MIS-11, whereas precession is more important during MIS-13. Obliquity being more important during MIS-11 and precession being more important during the interglacials of high eccentricity have also been found for other climate variables, such as surface air temperature, sea surface temperature and sea ice (Yin and Berger 2015; Wu et al. 2020).

To better understand the different responses of the F_{tree} to precession and obliquity between MIS-13 and MIS-11, we first compare the response of the F_{tree} to GDD0 and precipitation between the two interglacials. Fig. 7a shows that the response of the F_{tree} to GDD0 and precipitation during MIS-13 is very similar to that during MIS-11 (Fig. 4a) almost everywhere. Thus, the different response of the F_{tree} to precession and obliquity between MIS-13 and MIS-11 is mainly due to the different response of the GDD0 and precipitation to precession and obliquity during the two interglacials. The results of the F_{grass} are the same as the F_{tree} (Fig. 4b and Fig. 7b).

Fig. 8b shows that, similar to MIS-11(Fig. 5b), the GDD0 positively responds to both -precession and obliquity almost everywhere during MIS-13. However, as compared to MIS-11, the effect of precession on the GDD0 is more pronounced during MIS-13, while the effect of obliquity becomes weaker. The same happens to precipitation (Fig. 8a). Again, the different responses of the GDD0 and precipitation to precession and obliquity during the two interglacials are due to the difference in the precession and obliquity variations between the two interglacials as explained above.

3.4 Impacts of CO_2 on vegetation during MIS-11 and MIS-13

To investigate the influence of CO_2 on the vegetation composition during MIS-11 and MIS-13, the results of the second set of experiments (OrbGHG) are analyzed and compared with the first set of experiments (Orb). Fig. 9 shows that the impact of CO_2 on the F_{tree} is much less important than the astronomical parameters during both MIS-11 and MIS-13. As compared with Orb, CO_2 has no significant effect on the relative importance of precession and obliquity. However, the effect of CO_2 on the F_{tree} is slightly more important during MIS-13 than that during MIS-11 despite a lower CO_2 concentration, which can be explained by the fact that the amplitude of variation of CO_2 is higher during MIS-13, while the CO_2 concentration during most part of the MIS-11 simulation remains at a quite stable high level and is less varying (Fig. 1). Regarding the F_{grass} (Fig. 10), same as the astronomical parameters, the effect of CO_2 is nearly opposite to its effect on the F_{tree}. However, the relative importance of CO_2 on the F_{grass} during these two interglacials is the same as that on the F_{tree}.

To better understand the impact of CO_2 on the F_{tree} and F_{grass} during these two interglacials, we also investigated the response of the F_{tree} (Fig. S2) and F_{grass} (Fig. S3) to GDD0 and precipitation with OrbGHG and compared them with the results of Orb. The results show that the response of the F_{tree} and F_{grass} to GDD0 and precipitation have no obvious difference between these two sets of experiments during both MIS-11 and MIS-13 (Fig. 4 and Fig. 7). Thus, we further discuss the relationship between GDD0, precipitation and -precession, obliquity, CO_2 with OrbGHG.

Fig. S4 shows that the impact of CO_2 on the GDD0 is very small as compared to the astronomical parameters during MIS-11, with a slightly positive effect in the low latitudes of both hemispheres. However, the F_{tree} and F_{grass} have no obvious relationship with GDD0 in these regions because GDD0 is indeed always large there, and sensitivity studies show that the F_{tree} is much less sensitive to GDD0 when GDD0 is in a high level (Brovkin et al. 2002). The impact of CO_2 on precipitation is also very small in most regions as compared to the astronomical parameters during MIS-11. During MIS-13(Fig. S5), the spatial pattern of the relationship of CO_2 with GDD0 and precipitation is very similar to that during MIS-11, but with a stronger impact due to larger amplitude of variation of CO_2 during MIS-13. In particular, in South America, central-southern Africa, southern and eastern Asia as well as Australia, the impact of CO_2 on the GDD0 is much stronger than the impact of obliquity (Fig. S5). However, as the F_{tree} is insensitive to GDD0 in these regions (Fig. S2), it is insensitive to CO_2.

3.5 Half-precession signal in equatorial vegetation

Half-precession cycle is a unique feature in the equatorial insolation because the Sun passes the Equator twice a year so that the equatorial region receives maximum insolation twice during one precession cycle (Berger et al. 2006). This would lead to a strong half-precession signal in the climate variables that are sensitive to maximum insolation (Short et al. 1991). Half-precession cycle has indeed been recorded in some tropical proxy records, such as precipitation variations (Olago et al. 2000; Trauth et al. 2021) and lake-level fluctuations (Trauth et al. 2003; Thevenon et al. 2004). In this section, we will examine whether half-precession cycle also exists in our simulated vegetation over the lands near the Equator. For this, the first set of simulations where only insolation forcing is considered are used.

Fig.11 shows that during MIS-13, strong periodicity of ~10 ka exists in the simulated equatorial F_{tree}, and also in the annual mean precipitation and GDD0. Comparison with March and September monthly mean insolation at the Equator (10°N-10°S) shows that the half-precession signal in the simulated vegetation, precipitation and temperature is in good coherence with the maximum values of March/September monthly insolation, indicating that the half-precession signal in the simulated fields is a direct response to the maximum insolation at the Equator. Similar half-precession signal has also been found in the simulated sea surface temperature at the Equator during MIS-13 (Wu et al. 2020). These results show that the model is able to capture the half-precession signal resulting from the tropical insolation, reproduce it in precipitation and temperature and finally lead to half-precession cycle in the terrestrial vegetation. Different from MIS-13, the half-precession signal is very weak in the simulated vegetation and climate of MIS-11(Fig. 11), and it does not correspond well with the maximum insolation at the Equator. This is partly related to the relatively small variation of precession during MIS-11, which would lead to a weak impact of precession and therefore a weak half-precession signal in the tropics. However, this is probably not the only reason, because fourth-harmonic of precession signal has been found in the southwestern Iberia Mediterranean vegetation during MIS-19 (Sánchez Goñi et al., 2016), an interglacial which is also characterized by small variation of precession due to small eccentricity. In our additional simulation of MIS-19 (not shown in this study), half-precession signal occurs in the simulated equatorial vegetation although it is weaker than the half-precession signal in MIS-13. Although MIS-11 and MIS-19 both have small variation of precession, a major reason due to which they are considered as good astronomical analogue of the Holocene, one distinct difference is that the variation of obliquity during MIS-11 is much larger than that during MIS-19 and the Holocene (Yin and Berger, 2015). Therefore, the effect of precession is even more suppressed during MIS-11 due to its large variation of obliquity. The difference between MIS-13 and MIS-11 shows that the half-precession cycle is not stable in time. It is amplified when eccentricity is large leading to large variation in precession, and is suppressed when eccentricity is small and the variation of obliquity is large.

4. Conclusions

In this study, we performed two sets of transient simulations with only varied insolation and with varied insolation and GHGs, respectively, to investigate the impact of astronomical forcing and CO_2 on climate and vegetation changes during MIS-11 and MIS-13. Our results show that the impact of astronomical forcing and CO_2 have a diverse regional expression and different from one interglacial to another, which are characterized by a dominant effect of insolation on the global vegetation change, and CO_2 plays a relatively minor role. The response of climate variables (annual mean precipitation and GDD0) and vegetation cover is mainly controlled by precession during MIS-13 whilst by obliquity during MIS-11, which is consistent with some pollen records. The amplitude of precession variation is relatively large during MIS-13, which makes precession play a more important role in the GDD0 and precipitation during MIS-13 than that during MIS-11. In contrast, the amplitude of precession variation is very weak during MIS-11 and the one of obliquity is relatively large, which makes obliquity more important during MIS-11. Our simulations also reveal the half-precession signal in the equatorial annual mean precipitation and GDD0 as well as vegetation during MIS-13, as a direct response to the maximum insolation at the Equator. However, no obvious half-precession signal is simulated during MIS-11 due to the weak effect of precession and strong effect of obliquity. We would like to remind that in our simulations, only the effects of insolation and CO_2 are considered. In order to have a more comprehensive view on the forcings that drive vegetation evolution during MIS-11 and MIS-13, the impact of ice sheets will be presented in parallel in another paper, which will also allow a better and detailed comparison of the simulated vegetation with reconstructions at some key regions.

Acknowledgments

This work and Z.P. Wu are supported by the Fonds de la Recherche Scientifique-FNRS (F.R.S.-FNRS) under grant MIS F.4529.18. Q.Q. Su and A.Q. Lyu are supported by UCLouvain - China Scholarship Council Ph.D. co-funding fellowship (Grant #201704910855 and #201706190226). Q.Z. Yin is Research Associate of F.R.S.-FNRS. The authors thank Maria Sánchez Goñi for helpful discussions and two anonymous reviewers for their constructive comments. Computational resources have been provided by the supercomputing facilities of the Université catholique de Louvain (CISM/UCL) and the Consortium des Équipements de Calcul Intensif en Fédération Wallonie Bruxelles (CÉCI) funded by the Fond de la Recherche Scientifique de Belgique (F.R.S.-FNRS) under convention 2.5020.11.

References:

Berger A (1978) Long-Term Variations of Daily Insolation and Quaternary Clim. Changes. J Atmos Sci 35(12):2362-2367. doi:10.1175/1520-0469(1978)035<2362:LTVODI>2.0.CO;2

Berger A, Loutre MF, Yin QZ (2010) Total irradiation during any time interval of the year using elliptic integrals. Quat Sci Rev 29(17):1968-1982. doi:https://doi.org/10.1016/j.quascirev.2010.05.007

Berger A, Loutre MF (1991) Insolation values for the climate of the last 10 million years. Quat Sci Rev 10(4):297-317. doi:https://doi.org/10.1016/0277-3791(91)90033-Q

Berger A, Loutre MF, Mélice JL (2006) Equatorial insolation: from precession harmonics to eccentricity frequencies. Clim. Past 2(2):131-136. doi:10.5194/cp-2-131-2006

Bonis NR, Ruhl M, Kürschner WM (2010) Milankovitch-scale palynological turnover across the Triassic–Jurassic transition at St. Audrie's Bay, SW UK. J Geol Soc London 167(5):877-888. doi:10.1144/0016-76492009-141

Bosmans JHC, Drijfhout SS, Tuenter E, Hilgen FJ, Lourens LJ (2015) Response of the North African summer monsoon to precession and obliquity forcings in the EC-Earth GCM. Clim. Dyn. 44(1):279-297. doi:10.1007/s00382-014-2260-z

Bounceur N, Crucifix M, Wilkinson RD (2015) Global sensitivity analysis of the climate–vegetation system to astronomical forcing: an emulator-based approach. Earth Syst. Dynam. 6(1):205-224. doi:10.5194/esd-6-205-2015

Brovkin V (2002) Climate-vegetation interaction. J. Phys. IV France 12(10):57-72. Retrieved from https://doi.org/10.1051/jp4:20020452

Brovkin V, Bendtsen J, Claussen M, Ganopolski A, Kubatzki C et al (2002) Carbon cycle, vegetation, and Clim. Dyn. in the Holocene: Experiments with the CLIMBER-2 model. Global Biogeochemical Cycles 16(4):86-81-86-20. doi:10.1029/2001gb001662

Brovkin V, Ganopolski A, Svirezhev Y (1997) A continuous climate-vegetation classification for use in climate-biosphere studies. Ecol Modell 101(2):251-261. doi:10.1016/S0304-3800(97)00049-5

Claussen M, Fohlmeister J, Ganopolski A, Brovkin V (2006) Vegetation dynamics amplifies precessional forcing. Geophys. Res. Lett. 33:9709. doi:10.1029/2006GL026111

Coletti AJ, DeConto RM, Brigham-Grette J, Melles M (2015) A GCM comparison of Pleistocene super-interglacial periods in relation to Lake El'gygytgyn, NE Arctic Russia. Clim. Past 11(7):979-989. doi:10.5194/cp-11-979-2015

Cramer W, Bondeau A, Woodward FI, Prentice IC, Betts RA et al (2001) Global response of terrestrial ecosystem structure and function to CO_2 and climate change: results from six dynamic global vegetation models. Glob Chang Biol. 7(4):357-373. doi:10.1046/j.1365-2486.2001.00383.x

Crucifix M, Betts RA, Cox PM. (2005) Vegetation and climate variability: a GCM modelling study. Clim Dyn 24, 457–467. https://doi.org/10.1007/s00382-004-0504-z

Crucifix M, Betts RA, Hewitt CD (2005) Pre-industrial-potential and Last Glacial Maximum global vegetation simulated with a coupled climate-biosphere model: Diagnosis of bioclimatic relationships. Global and Planetary Change, 45(4), 295-312. https://doi.org/10.1016/j.gloplacha.2004.10.001

Crucifix M, Loutre FM (2002) Transient simulations over the last interglacial period (126–115 kyr BP): feedback and forcing analysis. Clim. Dyn. 19(5):417-433. doi:10.1007/s00382-002-0234-z

Dallmeyer A, Claussen M, Lorenz SJ, Sigl M, Toohey M, Herzschuh U (2021) Holocene vegetation transitions and their climatic drivers in MPI-ESM1.2. Clim. Past 17(6):2481-2513. doi:10.5194/cp-17-2481-2021

Droxler AW, Farrell JW (2000) Marine Isotope Stage 11 (MIS 11): new insights for a warm future. Glob. Planet. Change 24(1):1-5. doi:https://doi.org/10.1016/S0921-8181(99)00065-X

Dupont LM, Zhao X, Charles C, Faith JT, Braun D (2022) Continuous vegetation record of the Greater Cape Floristic Region (South Africa) covering the past 300,000 years (IODP U1479). Clim. Past 18(1):1-21. doi:10.5194/cp-18-1-2022

Dutton A, Carlson AE, Long AJ, Milne GA, Clark PU et al (2015) Sea-level rise due to polar ice-sheet mass loss during past warm periods. Science 349(6244):aaa4019. doi:10.1126/science.aaa4019

Fletcher WJ, Sánchez Goñi MF (2008) Orbital- and sub-orbital-scale climate impacts on vegetation of the western Mediterranean basin over the last 48,000 yr. Quaternary Research 70(3):451-464. doi:10.1016/j.yqres.2008.07.002

Giesecke T, Bennett K, Birks H, Bjune A, Bozilova E et al (2011) The pace of Holocene vegetation change – testing for synchronous developments. Quat Sci Rev 30:2805-2814. doi:10.1016/j.quascirev.2011.06.014

Goosse H, Brovkin V, Fichefet T, Haarsma R, Huybrechts P et al (2010) Description of the Earth system model of intermediate complexity LOVECLIM version 1.2. Geosci. Model Dev. 3(2):603-633. doi:10.5194/gmd-3-603-2010

Granoszewski W, Demske D, Nita M, Heumann G, Andreev AA (2005) Vegetation and climate variability during the Last Interglacial evidenced in the pollen record from Lake Baikal. Glob. Planet. Change 46(1):187-198. doi:https://doi.org/10.1016/j.gloplacha.2004.09.017

Guo ZT, Berger A, Yin QZ, Qin L (2009) Strong asymmetry of hemispheric climates during MIS-13 inferred from correlating China loess and Antarctica ice records. Clim. Past 5(1):21-31. doi:10.5194/cp-5-21-2009

Harrison SP, Kutzbach JE, Prentice IC, Behling PJ, Sykes MT (1995) The response of northern hemisphere extratropical climate and vegetation to orbitally-induced changes in insolation during the last interglaciation. Quaternary Research, 43 (2):174-184. doi:10.1006/qres.1995.1018

Harrison SP, Kutzbach JE, Liu Z, Bartlein PJ, Otto-Bliesner B et al (2003) Mid-Holocene climates of the Americas: a dynamical response to changed seasonality. Clim. Dyn. 20(7):663-688. doi:10.1007/s00382-002-0300-6

Helmke JP, Bauch HA, Röhl U, Kandiano ES (2008) Uniform climate development between the subtropical and subpolar Northeast Atlantic across marine isotope stage 11. Clim. Past 4(3):181-190. doi:10.5194/cp-4-181-2008

Hoegh-Guldberg O, Jacob D, Taylor M, Bindi M, Brown S et al (2018). Chapter 3: Impacts of 1.5°C global warming on natural and human systems. In: Global Warming of 1.5 °C. An IPCC special report on the impacts of global warming of 1.5 °C above preindustrial levels and related global greenhouse gas emission pathways [...]. In (pp. 175-311).

Jiménez-Moreno G, Aziz HA, Rodríguez-Tovar FJ, Pardo-Igúzquiza E, Suc JP (2007) Palynological evidence for astronomical forcing in Early Miocene lacustrine deposits from Rubielos de Mora Basin (NE Spain). Palaeogeogr. Palaeoclimatol. Palaeoecol. 252(3):601-616. doi:10.1016/j.palaeo.2007.05.013

Jahn, B, Schneider R, Muller PJ, Donner B, Röhl Ursula (2005) Response of tropical African and East Atlantic climates to orbital forcing over the last 1.7 Ma. Geological Society, London, Special Publications. 247. 65-84. 10.1144/GSL.SP.2005.247.01.04

Kleinen T, Hildebrandt S, Prange M, Rachmayani R, Müller S et al (2014) The climate and vegetation of Marine Isotope Stage 11 – Model results and proxy-based reconstructions at global and regional scale. Quat. Int. 348:247-265. doi:10.1016/j.quaint.2013.12.028

Kutzbach J, Liu, XD, Liu, ZY, Chen GS (2008) Simulation of the evolutionary response of global summer monsoons to orbital forcing over the past 280,000 years. Climate Dynamics. 30. 567-579. 10.1007/s00382-007-0308-z

Lang N, Wolff EW (2011) Interglacial and glacial variability from the last 800 ka in marine, ice and terrestrial archives. Clim. Past 7(2):361-380. doi:10.5194/cp-7-361-2011

Leemans R, Cramer WP (1991) The IIASA Database for Mean Monthly Values of Temperature, Precipitation, and Cloudiness on a Global Terrestrial Grid. IIASA Research Report. IIASA, Laxenburg, Austria: RR-91-018

Lieth, H (1975) Modeling the Primary Productivity of the World. In: Lieth, H., Whittaker, R.H. (eds) Primary Productivity of the Biosphere. Ecological Studies, vol 14. Springer, Berlin, Heidelberg. doi:10.1007/978-3-642-80913-2_12

Loutre MF, Berger A (2003) Marine Isotope Stage 11 as an analogue for the present interglacial. Glob. Planet. Change 36(3):209-217. doi:10.1016/S0921-8181(02)00186-8

Lüthi D, Floch M, Bereiter B, Blunier T, Barnola J-M et al (2008) High-resolution carbon dioxide concentration record 650,000-800,000 years before present. Nature 453:379-382. doi:10.1038/nature06949

Margari V, Roucoux K, Magri D, Manzi G, Tzedakis PC (2018) The MIS 13 interglacial at Ceprano, Italy, in the context of Middle Pleistocene vegetation changes in southern Europe. Quat Sci Rev 199:144-158. doi:https://doi.org/10.1016/j.quascirev.2018.09.016

Markovic S, Hambach U, Catto N, Jovanovic M, Buggle B et al (2009) Middle and Late Pleistocene loess sequences at Batajnica, Vojvodina, Serbia. Quat. Int. 198:255-266. doi:10.1016/j.quaint.2008.12.004

Markovic S, Hambach U, Stevens T, Jovanovic M, O'Hara-Dhand K et al (2012) Loess in the Vojvodina region (Northern Serbia): An essential link between European and Asian Pleistocene environments. Geologie en Mijnbouw 91:173-188. doi:10.1017/S0016774600001578

Masson-Delmotte V, Stenni B, Pol K, Braconnot P, Cattani O et al (2010) EPICA Dome C record of glacial and interglacial intensities. Quat Sci Rev 29:113-128. doi:10.1016/j.quascirev.2009.09.030

Mcmanus J, Oppo D, Cullen J, Healey S. (2003). Marine Isotope Stage 11 (MIS 11): Analog for Holocene and future climate? Washington DC American Geophysical Union Geophysical Monograph Series. 69-85. 10.1029/137GM06

Olago DO, Street-Perrott FA, Perrott RA, Ivanovich M, Harkness DD, Odada EO (2000) Long-term temporal characteristics of palaeomonsoon dynamics in equatorial Africa. Glob. Planet. Change 26(1):159-171. doi:https://doi.org/10.1016/S0921-8181(00)00041-2

Oliveira D, Desprat S, Rodrigues T, Naughton F, Hodell D et al (2016) The complexity of millennial-scale variability in southwestern Europe during MIS 11. Quaternary Research 86. doi:10.1016/j.yqres.2016.09.002

Oliveira D, Desprat S, Yin QZ, Naughton F, Trigo R et al (2018) Unraveling the forcings controlling the vegetation and climate of the best orbital analogues for the present interglacial in SW Europe. Clim. Dyn. 51(1):667-686. doi:10.1007/s00382-017-3948-7

Oliveira D, Desprat S, Yin QZ, Rodrigues T, Naughton F et al (2020) Combination of insolation and ice-sheet forcing drive enhanced humidity in northern subtropical regions during MIS 13. Quat Sci Rev 247:106573. doi:https://doi.org/10.1016/j.quascirev.2020.106573

Olson, J., Watts, J.A., 1992. Major World Ecosystem Complexes Ranked by Carbon in Live Vegetation: A Database. NDP-017, Oak Ridge National Laboratory, Oak Ridge, Tennessee, pp. 164

Pokras E, Mix A. (1987) Earth's precession cycle and Quaternary climatic change in tropical Africa. Nature 326, 486–487. https://doi.org/10.1038/326486a0

Prokopenko A, Bezrukova E, Khursevich G, Solotchina E, Kuzmin M (2009) Climate in continental interior Asia during the longest interglacial of the past 500 000 years: The new MIS 11 records from Lake Baikal, SE Siberia. Clim. Past Discuss. 6. doi:10.5194/cpd-5-1951-2009

Rachmayani R, Prange M, Michael S (2015) Intra-interglacial climate variability from Marine Isotope Stage 15 to the Holocene. Clim. Past Discuss. 11:3071-3107. doi:10.5194/cpd-11-3071-2015

Raymo ME, Mitrovica JX (2012) Collapse of polar ice sheets during the stage 11 interglacial. Nature 483(7390):453-456. doi:10.1038/nature10891

Russo Ermolli E, Di Donato V, Martín-Fernández JA, Orain R, Lebreton V, Piovesan G (2015) Vegetation patterns in the Southern Apennines (Italy) during MIS 13: Deciphering pollen variability along a NW-SE transect. Rev. Palaeobot. Palynol. 218:167-183. doi:https://doi.org/10.1016/j.revpalbo.2014.11.004

Sánchez Goñi MF, Landais A, Fletcher WJ, Naughton F, Desprat S, Duprat J. (2008) Contrasting impacts of Dansgaard-Oeschger events over a western European latitudinal transect modulated by orbital parameters. Quat. Sci. Rev. 27(11-12): 1136–1151. doi:10.1016/j.quascirev.2008.03.003

Sánchez Goñi MF, Teresa Rodrigues, David A. Hodell, Josue M. Polanco-Martinez, Montserrat Alonso-Garcia, Ivan Hernandez-Almeida, Stéphanie Desprat, and Patrizia Ferretti. "Tropically-driven climate shifts in southwestern Europe during MIS 19, a low eccentricity interglacial." Earth and Planetary Science Letters 448 (2016): 81-93.

Shi F, Yin QZ, Nikolova I, Berger A, Ramstein G, Guo ZT (2020) Impacts of extremely asymmetrical polar ice sheets on the East Asian summer monsoon during the MIS-13 interglacial. Quat Sci Rev 230:106164. doi:https://doi.org/10.1016/j.quascirev.2020.106164

Shichi K, Takahara H, Kawamuro K (2009) Vegetation and climate change during MIS 11 in southeastern Siberia based on pollen records from Lake Baikal sediment. Journal of Palynology 55:3-14.

Shin S-I, Sardeshmukh PD, Webb RS, Oglesby RJ, Barsugli JJ (2006) Understanding the Mid-Holocene Climate. J. Clim. 19(12):2801-2817. doi:10.1175/JCLI3733.1

Short DA, Mengel JG, Crowley TJ, Hyde WT, North GR (1991) Filtering of Milankovitch Cycles by Earth's Geography. Quaternary Research 35(2):157-173. doi:10.1016/0033-5894(91)90064-C

Stachowicz-Rybka R (2015) Vegetation of the Ferdynandovian interglacial (MIS 13–15) based on plant macrofossils from a new profile of the stratotype site. Acta Palaeobotanica 55. doi:10.1515/acpa-2015-0011

Sun YB, Yin QZ, Crucifix M, Clemens SC, Araya-Melo P et al (2019) Diverse manifestations of the mid-Pleistocene climate transition. Nat. Commun. 10(1):352. doi:10.1038/s41467-018-08257-9

Tarasov P, Bezrukova E, Karabanov E, Nakagawa T, Wagner M et al (2007) Vegetation and Clim. Dyn. during the Holocene and Eemian interglacials derived from Lake Baikal pollen records. Palaeogeogr. Palaeoclimatol. Palaeoecol. 252:440-457. doi:10.1016/j.palaeo.2007.05.002

Tarasov P, Bezrukova E, Krivonogov S (2009) Late Glacial and Holocene changes in vegetation cover and climate in southern Siberia derived from a 15 kyr long pollen record from Lake Kotokel. Clim. Past 5(3):285-295. doi:10.5194/cp-5-285-2009

Tarasov PE, Andreev AA, Anderson PM, Lozhkin AV, Leipe C et al (2013) A pollen-based biome reconstruction over the last 3.562 million years in the Far East Russian Arctic - new insights into climate-vegetation relationships at the regional scale. Clim. Past 9(6):2759-2775. doi:10.5194/cp-9-2759-2013

Thevenon F, Bard E, Williamson D, Beaufort L (2004) A biomass burning record from the West Equatorial Pacific over the last 360 ky: methodological, climatic and anthropic implications. Palaeogeogr. Palaeoclimatol. Palaeoecol. 213(1):83-99. doi:https://doi.org/10.1016/j.palaeo.2004.07.003

Trauth MH, Asrat A, Cohen AS, Duesing W, Foerster V et al (2021) Recurring types of variability and transitions in the ~620 kyr record of climate change from the Chew Bahir basin, southern Ethiopia. Quat Sci Rev 266:106777. doi:https://doi.org/10.1016/j.quascirev.2020.106777

Trauth MH, Deino AL, Bergner AGN, Strecker MR (2003) East African climate change and orbital forcing during the last 175 kyr BP. Earth Planet. Sci. Lett. 206(3):297-313. doi:https://doi.org/10.1016/S0012-821X(02)01105-6

Tuenter E, Weber SL, Hilgen FJ, Lourens LJ (2003) The response of the African summer monsoon to remote and local forcing due to precession and obliquity. Glob. Planet. Change 36(4):219-235. doi:https://doi.org/10.1016/S0921-8181(02)00196-0

Tzedakis PC, Roucoux KH, De Abreu L, Shackleton N J (2004) The duration of forest stages in southern Europe and interglacial climate variability. Science, 306(5705), 2231-2235. doi: 10.1126/science.1102398

Tzedakis PC (2005) Towards an understanding of the response of southern European vegetation to orbital and suborbital climate variability. Quat Sci Rev 24(14):1585-1599. doi:https://doi.org/10.1016/j.quascirev.2004.11.012

Tzedakis PC (2010) The MIS 11 - MIS 1 analogy, southern European vegetation, atmospheric methane and the "early anthropogenic hypothesis". Clim. Past 6(2):131-144. doi:10.5194/cp-6-131-2010

Tzedakis PC, Hooghiemstra H, Pälike H (2006) The last 1.35 million years at Tenaghi Philippon: revised chronostratigraphy and long-term vegetation trends. Quat Sci Rev 25(23):3416-3430. doi:https://doi.org/10.1016/j.quascirev.2006.09.002

Vogel H, Meyer-Jacob C, Melles M, Brigham-Grette J, Andreev AA et al (2013) Detailed insight into Arctic climatic variability during MIS 11c at Lake El'gygytgyn, NE Russia. Clim. Past 9(4):1467-1479. doi:10.5194/cp-9-1467-2013

Willeit M, Ganopolski A, Feulner G (2013) On the effect of orbital forcing on mid-Pliocene climate, vegetation and ice sheets. Clim. Past 9(4):1749-1759. doi:10.5194/cp-9-1749-2013

Williams JW, Shuman B, Bartlein PJ, Diffenbaugh NS, Webb T, III (2010) Rapid, time-transgressive, and variable responses to early Holocene midcontinental drying in North America. Geology 38(2):135-138. doi:10.1130/G30413.1

Wu ZP, Yin QZ, Guo ZT, Berger A (2020) Hemisphere differences in response of sea surface temperature and sea ice to precession and obliquity. Glob. Planet. Change 192:103223. doi:10.1016/j.gloplacha.2020.103223

Wyrwoll K-H, Liu ZY, Chen GS, Kutzbach JE, Liu XD (2007) Sensitivity of the Australian summer monsoon to tilt and precession forcing. Quat Sci Rev 26(25):3043-3057. doi:https://doi.org/10.1016/j.quascirev.2007.06.026

Yin QZ, Berger A (2012) Individual contribution of insolation and CO_2 to the interglacial climates of the past 800,000 years. Clim. Dyn. 38:709-724. doi:10.1007/s00382-011-1013-5

Yin QZ, Berger A (2015) Interglacial analogues of the Holocene and its natural near future. Quat Sci Rev 120. doi:10.1016/j.quascirev.2015.04.008

Yin QZ, Guo ZT (2006) Mid-Pleistocene vermiculated red soils in southern China as an indication of unusually strengthened East Asian monsoon. Chinese Science Bulletin 51:213-220. doi:10.1007/s11434-005-0490-5|ISSN

Yin QZ, Guo ZT (2008) Strong summer monsoon during the cool MIS-13. Clim. Past 4(1):29-34. doi:10.5194/cp-4-29-2008

Yin QZ, Wu ZP, Berger A, Goosse H, Hodell D (2021) Insolation triggered abrupt weakening of Atlantic circulation at the end of interglacials. Science 373(6558):1035-1040. doi:10.1126/science.abg1737

Zhao Y, Tzedakis Polychronis C, Li Q, Qin F, Cui QY et al (2020) Evolution of vegetation and climate variability on the Tibetan Plateau over the past 1.74 million years. Science Advances 6(19):eaay6193. doi:10.1126/sciadv.aay6193

Zhao Y, Yu ZC, Herzschuh U, Yang B, Zhao H et al (2014) Vegetation and climate change during Marine Isotope Stage 3 in China. Chinese Science Bulletin 59(33):4444-4455. doi:10.1007/s11434-014-0611-0

Statements and Declarations

Funding

This work was supported by the Fonds de la Recherche Scientifique-FNRS (F.R.S.-FNRS) under grant MIS F.4529.18. Q.Q. Su and A.Q. Lyu, are supported by China Scholarship Council (CSC) Grant #201704910855 and #201706190226. Q.Z. Yin is Research Associate of F.R.S.-FNRS. Computational resources have been provided by the supercomputing facilities of the Université catholique de Louvain (CISM/UCL) and the Consortium des Équipements de Calcul Intensif en Fédération Wallonie Bruxelles (CÉCI) funded by the Fond de la Recherche Scientifique de Belgique (F.R.S.-FNRS) under convention 2.5020.11.

Competing Interests

The authors have no relevant financial or non-financial interests to disclose.

Author Contributions

Q.Q. Su and A.Q. Lyu contributed to the analysis of the results and the writing of the first draft of the paper. Z.P. Wu performed the model simulations. Q.Z. Yin contributed to the conception, design and supervision of the study. All authors contributed to the discussion of the results and the writing of the final manuscript.

Data Availability

The datasets analyzed in the current study are available from the corresponding author on reasonable request.

Figure

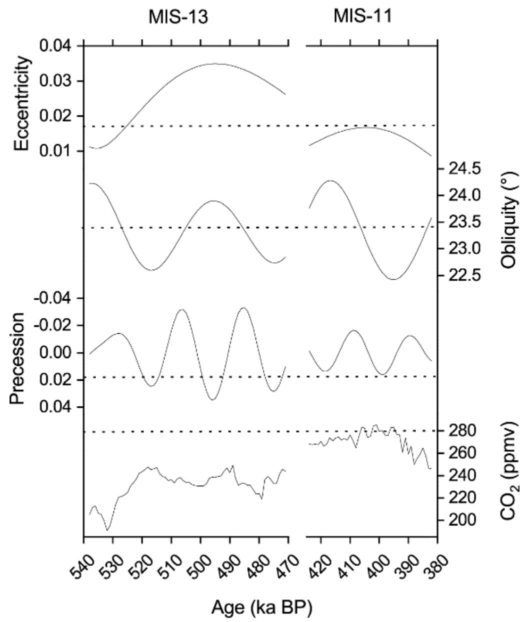

Fig. 1 Astronomical parameters (Berger and Loutre, 1991) and atmospheric CO_2 concentration (Lüthi et al. 2008) used in the simulations for MIS-13 and MIS-11. Dotted lines indicate Pre-Industrial values.

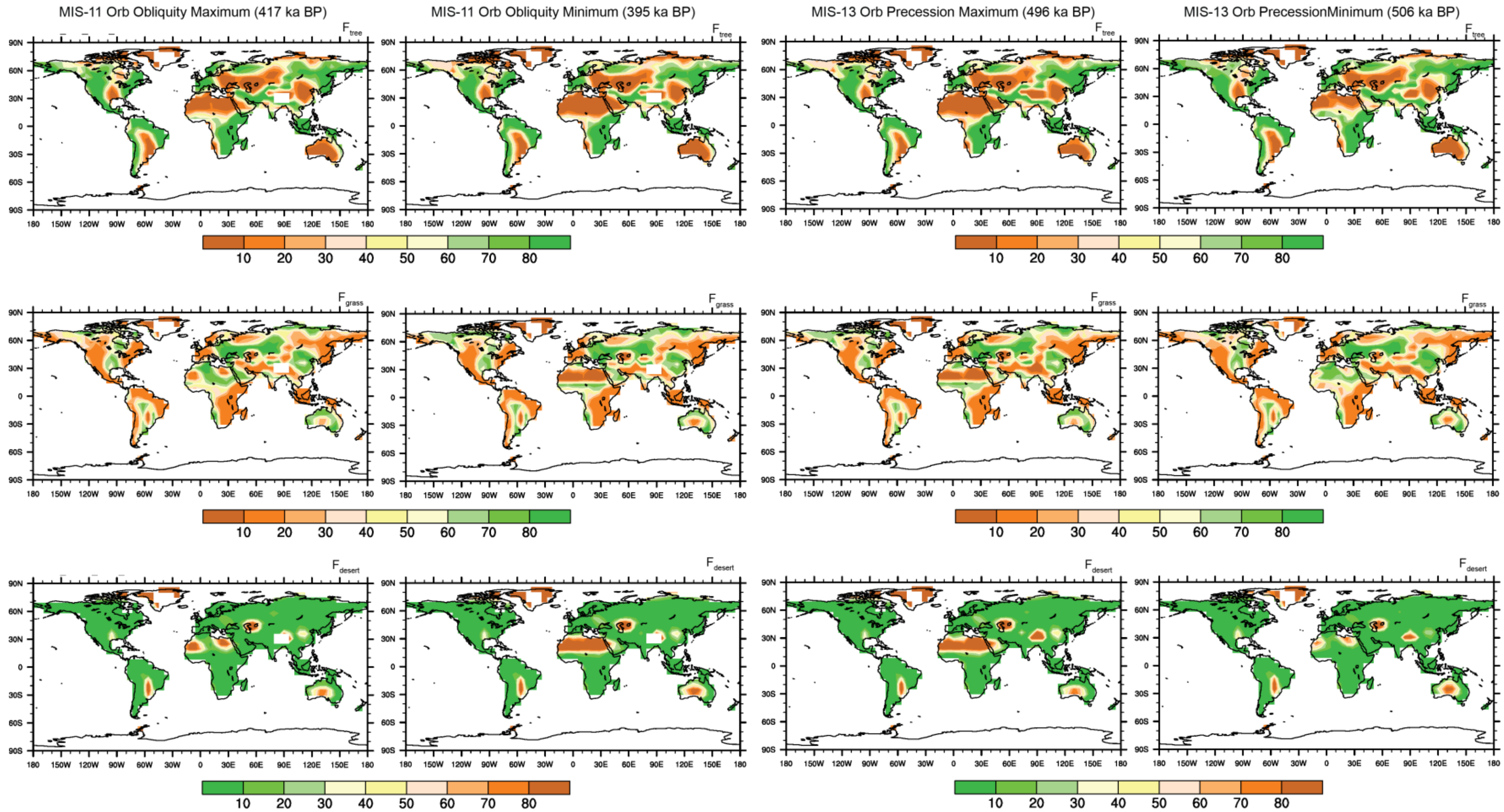

Fig. 2 Global map of the F_{tree}, F_{grass} and F_{desert} under four extreme astronomical conditions: maximum and minimum obliquity conditions (417 kaBP and 395 kaBP respectively) during MIS-11 in Orb (forced by Orbital parameters only) experiment, and maximum and minimum precession conditions (496 kaBP and 506 kaBP respectively) during MIS-13 in Orb experiment.

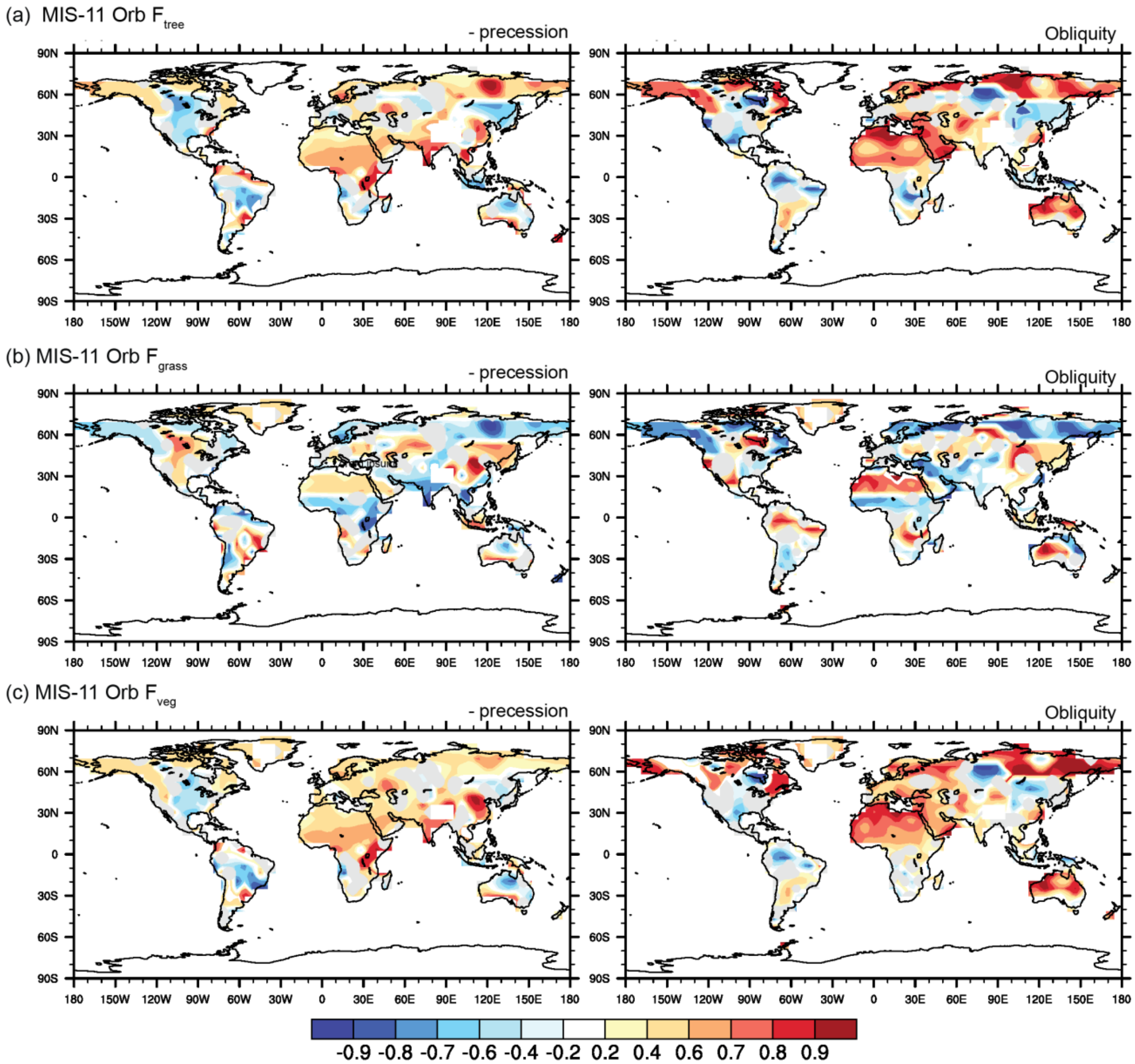

Fig. 3 Multi-linear regression coefficient maps of F_{tree} (a), F_{grass} (b) and F_{veg} (c) related to the -precession and obliquity during MIS-11 in Orb experiment. Regions where the respective coefficient is not statistically significant ($p < 0.05$) are grey shaded.

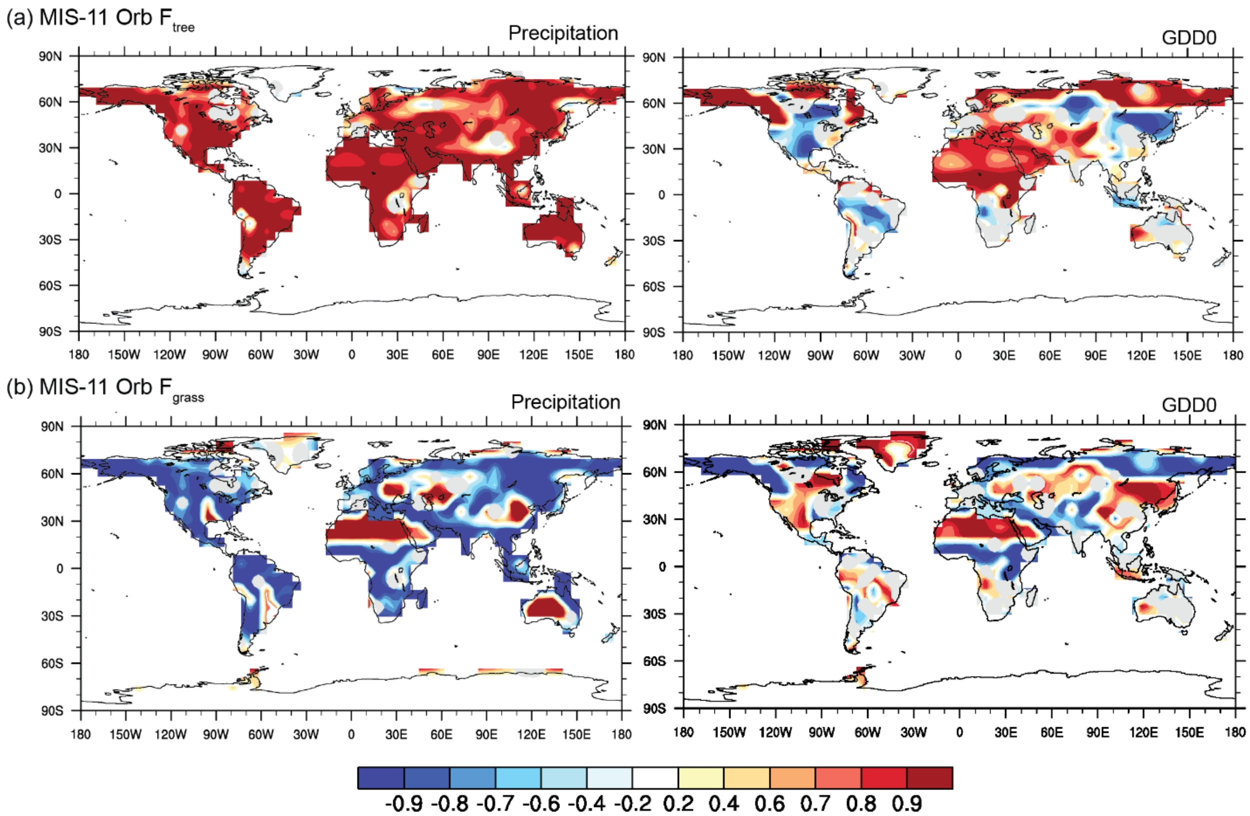

Fig. 4 Simple linear regression coefficient maps of F_{tree} (a) and F_{grass} (b) related to the annual mean precipitation and GDD0 during MIS-11 in Orb experiment. Regions where the respective coefficient is not statistically significant ($p < 0.05$) are grey shaded.

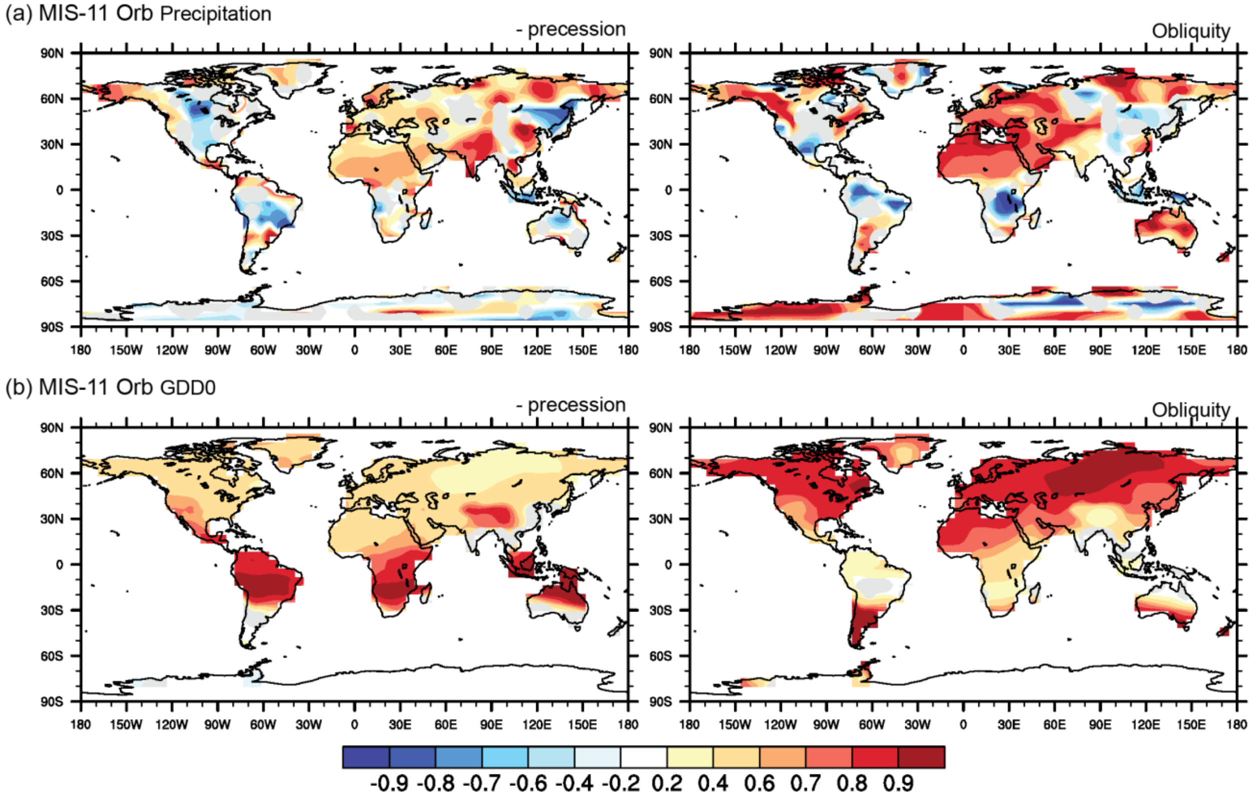

Fig. 5 Multi-linear regression coefficient maps of the annual mean precipitation (a) and GDD0 (b) related to -precession and obliquity during MIS-11 in Orb experiment. Regions where the respective coefficient is not statistically significant ($p < 0.05$) are grey shaded.

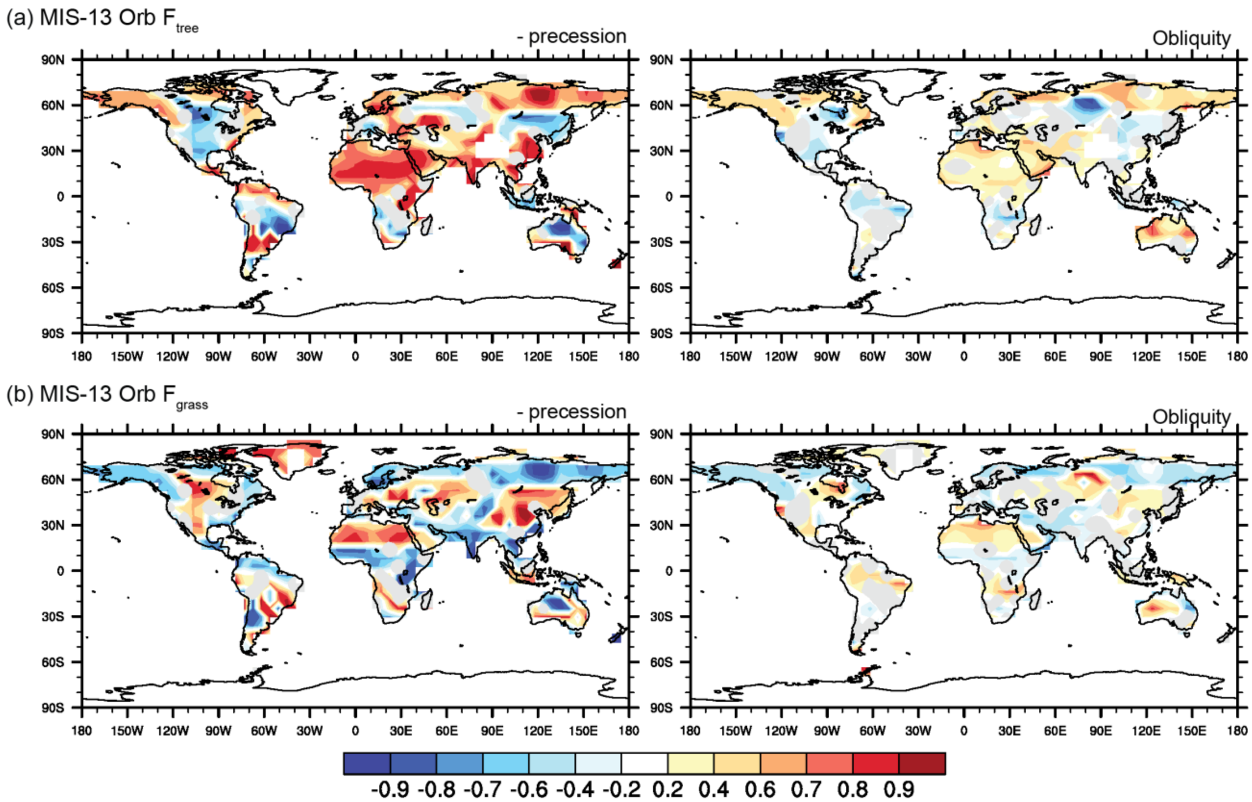

Fig. 6 Multi-linear regression coefficient maps of F_{tree} and F_{grass} related to the -precession and obliquity during MIS-13 in Orb experiment. Regions where the respective coefficient is not statistically significant ($p < 0.05$) are grey shaded.

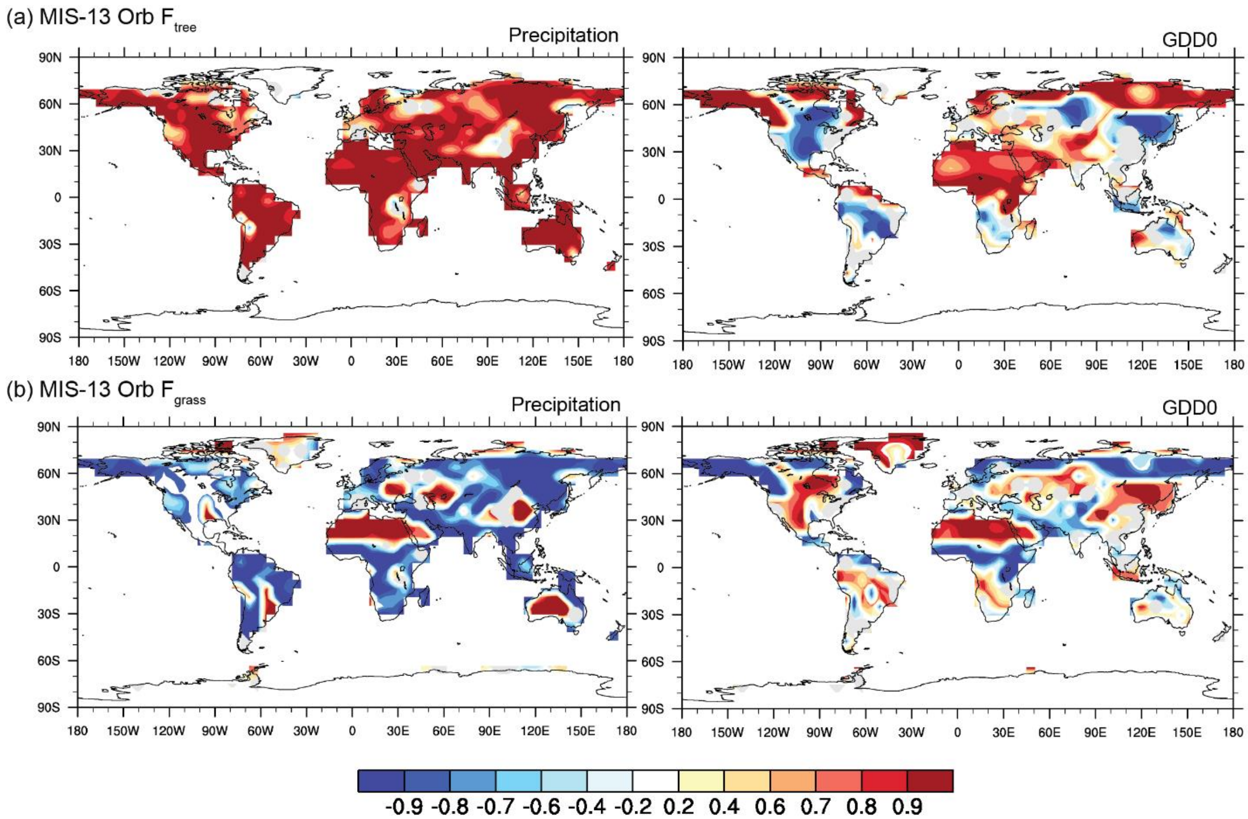

Fig. 7 Simple linear regression coefficient maps of F_{tree} (a) and F_{grass} (b) related to the annual mean precipitation and GDD0 during MIS-13 in Orb experiment. Regions where the respective coefficient is not statistically significant ($p < 0.05$) are grey shaded.

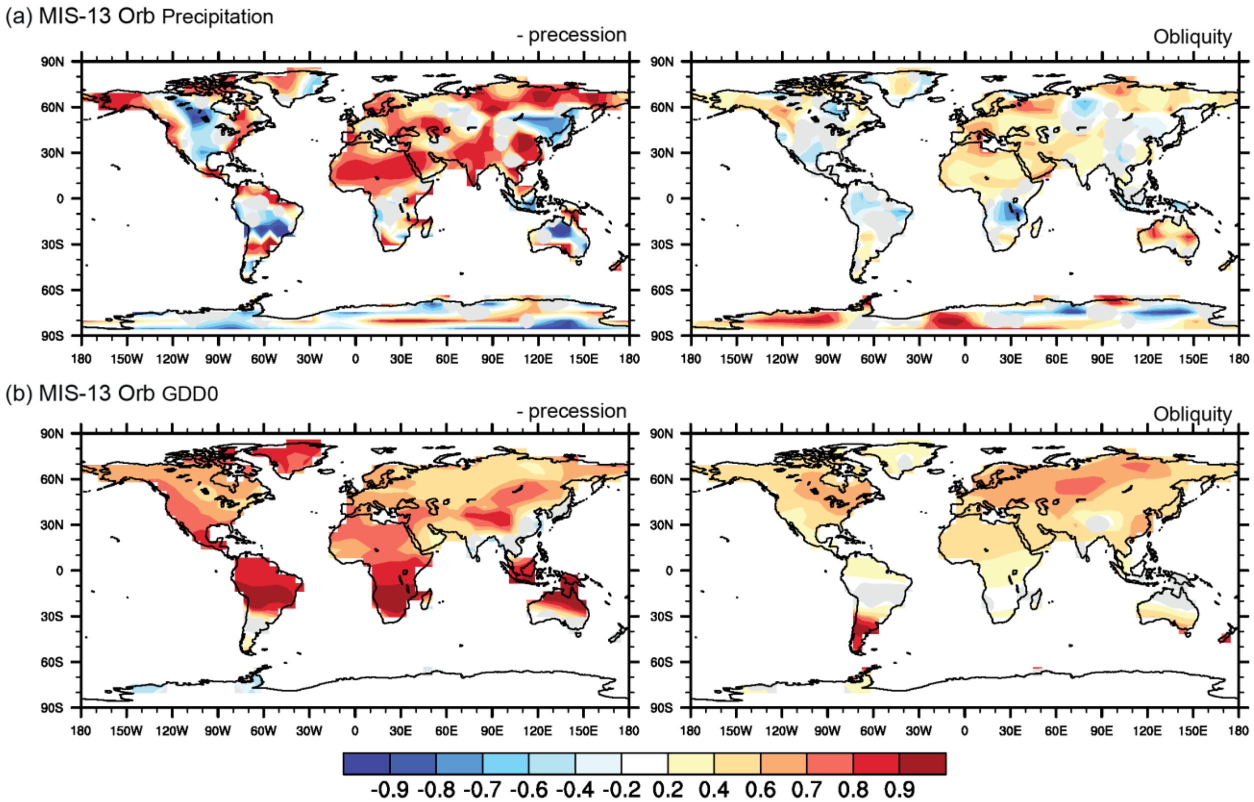

Fig. 8 Multi-linear regression coefficient maps of the annual mean precipitation (a) and GDD0 (b) related to -precession and obliquity during MIS-13 in Orb experiment. Regions where the respective coefficient is not statistically significant ($p < 0.05$) are grey shaded.

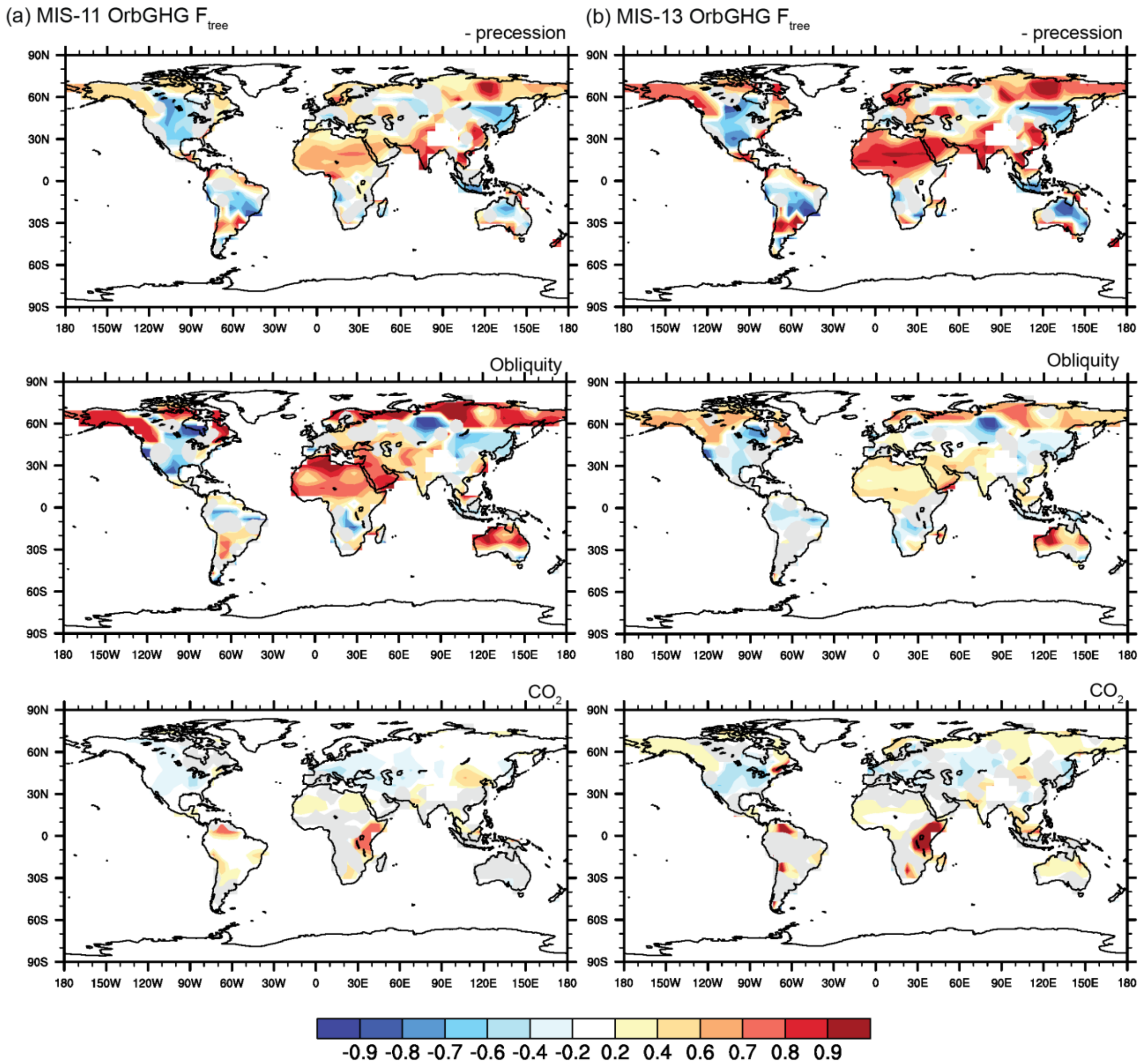

Fig. 9 Multi-linear regression coefficient maps of F_{tree} related to the -precession, obliquity and CO_2 during MIS-11 (a) and MIS-13 (b) in OrbGHG (forced by Orbital parameters and GreenHouse Gas) experiment. Regions where the respective coefficient is not statistically significant ($p < 0.05$) are grey shaded.

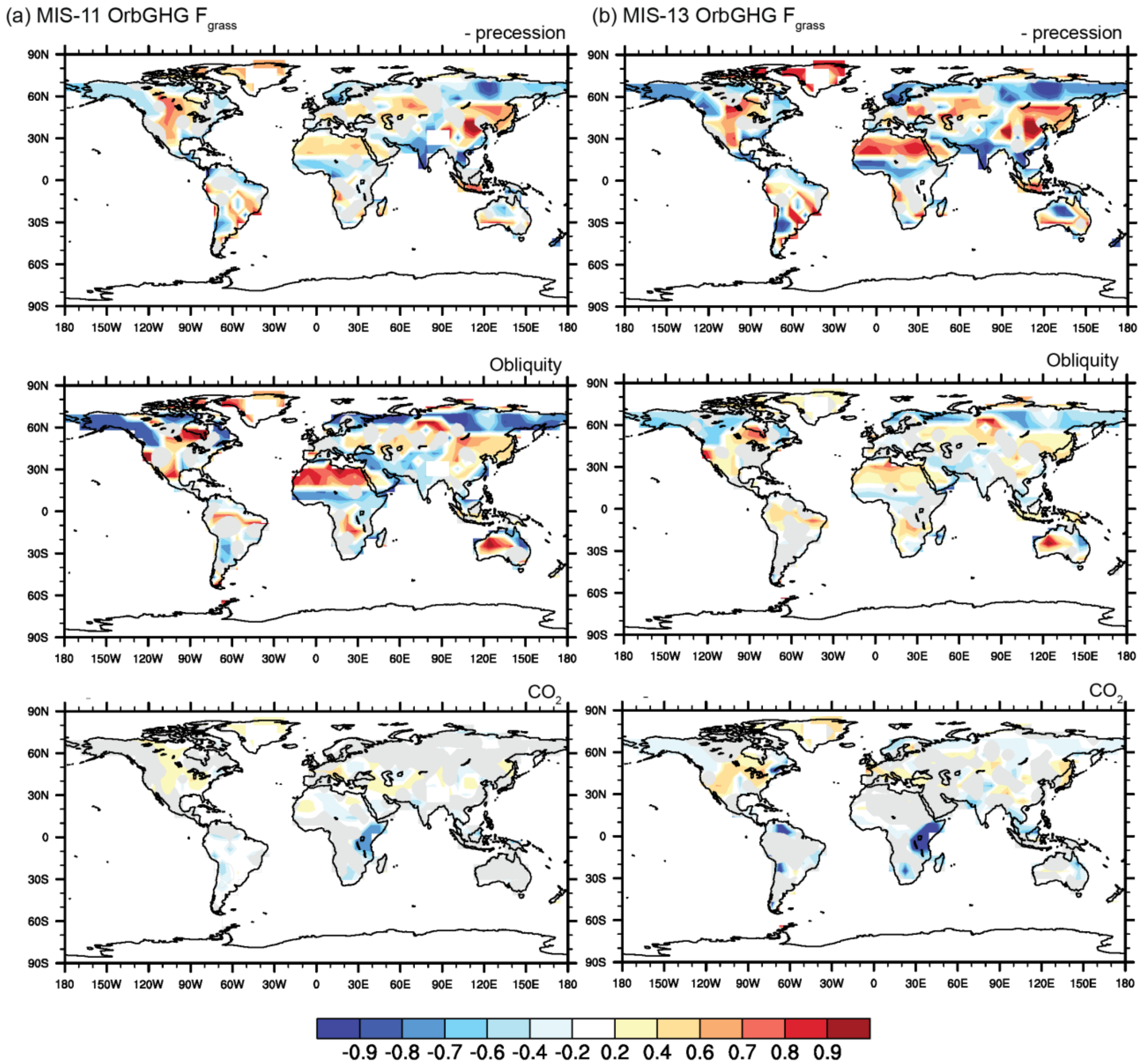

Fig. 10 Multi-linear regression coefficient maps of F_{grass} related to the -precession and obliquity and CO_2 during MIS-11 (a) and MIS-13 (b) in OrbGHG experiment. Regions where the respective coefficient is not statistically significant ($p < 0.05$) are grey shaded.

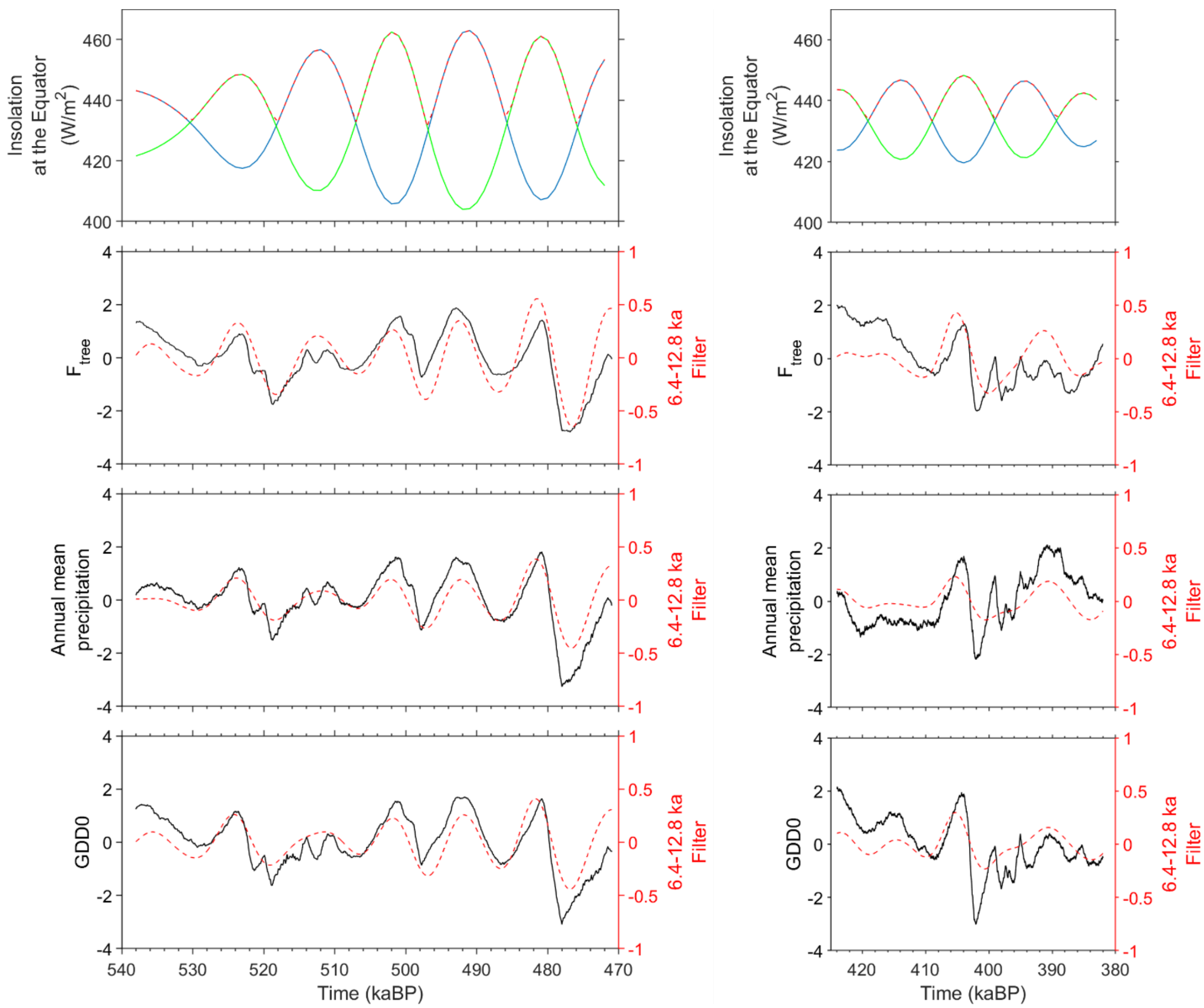

Fig. 11 Comparison between insolation and half precession signal at the Equator (10°N-10°S) during MIS-13 and MIS-11. Blue lines indicate the monthly mean insolation in March, green lines indicate the monthly mean insolation in September, the maximum values of these two are in red dashed lines. Black lines indicate the detrended data of F_{tree}, precipitation and GDD0 (standardized and 1 ka running mean) by a 12.8ka high pass filter. Red dashed lines indicate Gaussian 6.4 -12.8 ka filter.